Nanometer Effect Promoting Arsenic Removal on α-MnO2 Nano-surface in Aqueous Solution: DFT+U Research

Guifa Li (lgf_918@126.com)
Nanchang Hangkong University
Pengsen Zhao
Nanchang Hangkong University
Haizhong Zheng
Nanchang Hangkong University
Lixia Yang
Nanchang Hangkong University
Yongxiang Geng
Nanchang Hangkong University
Ping Peng
Hunan University

Research Article

Keywords: Arsenic irons, MnO2 nano-surface, catalytic mechanism, transitional product, DFT+U method

Posted Date: March 4th, 2021

DOI: https://doi.org/10.21203/rs.3.rs-220582/v1

Version of Record: A version of this preprint was published at Environmental Science and Pollution Research on July 29th, 2021. See the published version at https://doi.org/10.1007/s11356-021-15586-8.

Nanometer effect promoting arsenic removal on α-MnO_2 nano-surface in aqueous solution: DFT+U research

Guifa Li[1], Pengsen Zhao[1], Haizhong Zheng[1,2*], Lixia Yang[3], Yongxiang Geng[1], Ping Peng[4]

[1]*School of Material Science and Engineering, Nanchang Hangkong University, Jiangxi 330063, China*

[2]*Jiangxi Provincial Engineering Research Center for Surface Technology of Aeronautical Materials, Nanchang Hangkong University, Jiangxi 330063, China*

[3]*High Level Laboratory of Jiangxi Province for Persistent Pollutants Control, Recycle and Reuse, Nanchang Hangkong University, Nanchang 330063, PR China*

[4]*School of Material Science and Engineering, Hunan University, Hunan 410082, China*

[*] Corresponding author: zhznchu@126.com(H.Zheng)

Abstract: The nanometer effect in the process of arsenic ions removal on α-MnO_2 nano-surface is studied by first-principles method through microfacet models. Several parameters, such as adhesion energy, electrostatic potential, Mulliken population were calculated to illuminate the internal mechanism. The results show that the adsorption energies of $As(OH)_3$ molecules on MnO_2[(100×110)] nanostructure are smaller than that on bulk surface with the same concentration, which means the nanometer effect is beneficial to enhance the adsorption ability of MnO_2 nano-surface. In aqueous solution, there exist two possible removal ways of As ions. One is the direct reaction of $As(OH)_3 \rightarrow As(OH)_6^-$, which occurs both in bulk surface and nano-surface. However to nanomaterials, there exists another removal way of $As(OH)_3 \rightarrow As(OH)_4 \rightarrow As(OH)_6^-$ through an intermediate $As(OH)_4$ molecule produced by nanometer effect. Furthermore the smaller electrostatic potential of As ions on [(100×110)] nano-surface is beneficial to enhance the removal capability of As ions. Then the reason why MnO_2 nanomaterials have better catalytic activity than the bulk materials is originated from its much less adhesion energy, much more removal ways and much smaller electrostatic potential. So this research provides a detailed understanding on the removal capability of toxic ions influenced by nanometer effect.

Keywords: Arsenic irons; MnO_2 nano-surface; catalytic mechanism; transitional product; DFT+U method

1. Introduction

The arsenic contamination of groundwater has brought a great impact on human life (Jomova et al. 2011; Chandra et al. 2010), which is why the removal of arsenic has become one of the hotspots in human social research. Traditional technologies of arsenic removal, such as coagulation-filtration (Gupta and Ghosh 2009), ion exchange (Pessoa-Lopes et al. 2016) and other methods (Xiao et al. 2015), have high operating costs, which can't satisfy the large-scale needs of human beings. Thus the adsorption technology, which is economical and efficient, becomes the prior choice (Mishra and Ramaprabhu 2011). α-MnO_2 with a 2×2 tunnel structure (Xiao et al. 2009), owns good catalytic performance and can effectively degrade toxic organic pollutants (Li et al. 2014). It can effectively remove toxic metallic ions from the water via adsorption process (Gheju et al. 2016), which becomes a

good candidate material to remove arsenic. Thanh et al. (2012) have synthesized some α-MnO_2 nanorods through ball-milling of a physical blend and an in situ formation of laterite. He finds that their adsorption capacities (9.7mg/g) for arsenate (As(V) are affected by highly pH dependent and adsorption kinetics. Zhang and Sun (2013) have investigated the As removal capacity of α-MnO_2 dandelion like microspheres and point out that the arsenite (As(III)) species can be effectively oxidized by synthesized MnO_2 nanomaterials followed by the adsorption of As(V) species. Their adsorption capacities for As(V) ions increase to 14.5mg/g. Luo et al. (2018) have discussed the influence of pH and solvent (NaF, NaCl, Na_2SO_4) on the arsenic adsorption of α-MnO_2 nanofibers and find that the adsorption capacity of As(III) and As(V) ions enhances sharply to 117.72 mg/g and 60.19 mg/g, respectively. During the oxidation of As(III)→As(V) ions in the adsorption process, trace As(IV) ions appear in experimental research (Sun et al. 2015; Klaening et al. 1989). Some Mn(IV) ions are also reduced to Mn(III) ions and even Mn (II) ions to dissolve (Zhang and Sun 2013; Ge et al. 2016). So all of them find the MnO_2 nanomaterials have excellent arsenic adsorption capacity. But the internal mechanism of nanometer effect still keeps mysterious. To explore this problem, Luo et al. (2018) point out the As(III) and As(V) ions on MnO_2(100) surface are more stable than that on MnO_2(110) surface, and the strong As(III) emoval ability of α-MnO_2 nanofibers originates from its large adhesion energy by density functional theory (DFT) method. Zhang et al. (2015) have investigated the As(IV) adsorption ability on TiO_2 (001) and TiO_2(110) bulk surface, and reveal that the TiO_2(110) plane has a higher affinity toward arsenate than the TiO_2(001). α-MnO_2 nanomaterials may have many active sites such as steps, ledges, kinks and vacancy. Such chemical active sites are much more vigorous than that of bulk surface (Chen et al. 2017). Chen et al. (2017) have investigated chemical property of α-MnO_2 nanorod through bulk surface and microfacet with nanostructure by DFT, and find that the surface energy of microfacet is larger than that of the bulk surface. The junction of different Miller index in nanomaterials is the chemical active site. Then using bulk surface model to investigate the chemical property of nanomaterial has its own limits (Jiao and Bruce 2007). Furthermore the formation process of metastable valance state As(IV) ion keeps still mysterious right now. Using microfacet with nanostructure, the formation mechanism of $Sb(OH)_4^-$ precursor product is illuminated in detail (Li et al. 2018). Thus this paper is to explore the nanometer effect of α-MnO_2 nano-surface influence on the adsorption/desorption processes of arsenic ions and to discover the catalytic mechanism of metastable As^{4+} by DFT + U method.

2. Simulation models and method

For α-MnO_2 nanoparticles, its nano-surface is mainly composed by {110} and {100} Miller indexes (Reddy et al. 2009; Tompsett et al. 2014a). Then its corner nanostructure simulated by [(100×110)] microfacet model. For

comparison, the corresponding (100) and (110) bulk surfaces were also built as shown in Fig.1. To investigate the adsorption/desorption ability of arsenic ions in solution environment, different concentrations of $As(OH)_3$ or $As(OH)_6^-$ surrounded by several water molecules were constructed as shown in Fig. 1. To distinguish different concentration and adsorption sites of $As(OH)_3$ or $As(OH)_6^-$ molecules, the Roman numbers as I, II, III, …represent different adsorption sites and Arabic numbers as 1, 2, 3, …represent the numbers of arsenic molecules. For example, (100)-3As(III) indicates that there exist three $As(OH)_3$ molecule locating at (I), (II) and (III) sites respectively. The detailed adsorption/desorption models of As ions on MnO_2 surface are shown in Fig. S1.

The calculated models in this paper were optimized by DFT embedded in Cambridge Sequential Total Energy Package (CASTEP) code with plane waves and pseudopotentials (Luo et al. 2018; Song et al. 2018; Segall et al. 2002). A generalized gradient approximation (GGA) incorporated with Perdew, Burke, and Ernzerh with Hubbard U correction was used to treat their electronic structure to get globally stable structure (Xin et al. 2015; Youmbi and Calvayrac 2014). The cut-off energy of all simulation models was set at 450 eV and *K* point was set as 1×2×1 in the Brillouin zone of supercell models. The Broyden-Fletcher-Goldfarb-Shanno (BFGS) scheme (Tompsett et al. 2014a) was used to adjust the convergence criterions as root-mean-square (RMS) force (0.1 eV/Å), stress of 0.2 GPa and displacement of 0.005 Å (Chen et al. 2017)]. The energy tolerance was set to 5×10^{-4} eV/atom and the convergence criteria of self consistent field (SCF) was set to 1.0×10^{-4}.

Previous work has shown that DFT+U can well describe the structural stability, band gap and magnetic interaction when the fully-localized limit (Chen et al. 2017), which is the reason for our application in this study. The Hubbard U value is set to 1.6 eV to correct 3*d* orbital electronic structure of Mn atoms (Luo et al. 2018). The calculated lattice constants of α-MnO_2 obtained from DFT + U are listed in Table S1. And these results are within 1.8% of the theoretical (Luo et al. 2018; Tompsett et al. 2014b) and experimental (Johnson et al. 1997; Li et al. 2011) determined lattice parameters, indicating that DFT + U is reliable to evaluate the unit cell volume. The lattice constants of initial α-MnO_2 cell are a=b=9.922 Å and c = 2.904Å. All of these surface models were constructed from the optimized globally α-MnO_2 crystal.

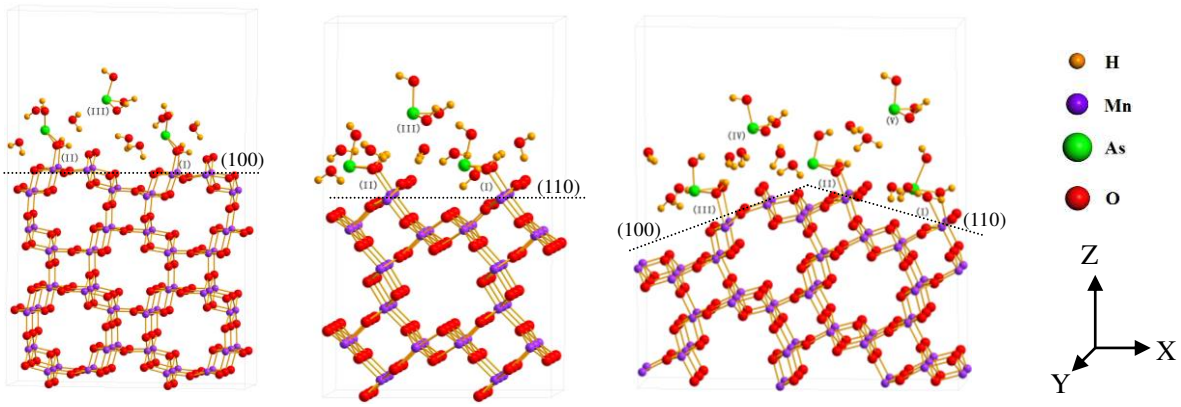

(a) (b) (c)

Fig. 1 Adsorption models of $As(OH)_3$ molecules with different concentration and sites on (a) (100), (b) (110) bulk surface and (c) [(100×110)] microfacet.

3. Results and discussion

3.1 Removal ability of bulk surface

Luo et al. (2018) have pointed out the surface complexes of As(III) and As(V) on (100) are more stable than (110), and electrons transfer from As(III) on (100) is greater than that on (110). But he doesn't consider the influence of As ions concentration. In this paper, the effect of $As(OH)_3$ concentration in aqueous solution is considered further. In order to study the difference in arsenic adsorption between bulk surface and nano-surface, the adsorption energy (E_{ad}) of As ions with different concentrations were calculated as following equation (Li et al. 2018):

$$E_{ad} = E_{surface+As} - E_{surface} - n \times E_{As} - m \times E_{H_2O} \quad (1)$$

wherein $E_{surcafe+As}$ means that the total energy of MnO_2 bulk or micofacet models with some As molecules in aqueous solution. $E_{surface}$ presents that the total energy of MnO_2 bulk or micofacet models. E_{As} and E_{H_2O} represent the energies of the As molecule and H_2O molecule, which are equal to -2187.203 eV and -469.78 eV, respectively. Wherein a $10\times10\times10$ ($Å^3$) vacuum box was built with only one $As(OH)_3$ or H_2O molecule at the center of the box to calculate their energy at gas state. And n and m mean the number of H_2O and $As(OH)_3$ molecules in the simulated system. The results are shown in Table 1 and Fig. S2. It is found that the adsorption energy of (100)-As(I) (concentration equal to 19.69mg/g) is E_{ad} = -2.641 eV. The adsorption energy of (100)-2As(II) with two $As(OH)_3$ molecules (concentration equal to 39.34mg/g) is E_{ad} = -6.05 eV, which is larger than the adsorption energy of (100)-As(I). But the adsorption energy of (100)-3As(III) with three $As(OH)_3$ molecules is E_{ad} = -6.396 eV, which is less than the three times adsorption energy of (100)-As(I). That is because the third $As(OH)_3$ molecule doesn't be adsorbed on the surface layer of (100). Its little difference in adsorption energy compared with (100)-2As(II) comes from the mutual effect of $As(OH)_3$ molecules. Analyzed the Mn atoms along surface layer of (100) bulk surface, it is found that there exist two adsorbed sites for $As(OH)_3$ molecules on each up layer and down layer as shown in Fig. 1. Considering the periodic symmetry of bulk surface model, the maximum adsorption capacity of (100) bulk surface is quadruple to that of the (100)-As(I), which is equal to 78.67 mg/g. The evolution of adsorption energies in (110)-$As(OH)_3$ system is consistent with that in (100)-$As(OH)_3$. The adsorption energy of (110)-2As(II) (E_{ad}=-4.892 eV) with two $As(OH)_3$ molecules is larger than the double adsorption energy of (110)-As(I) (E_{ad}=-2.401 eV). The adsorption energy of (110)-3As(III) (E_{ad} = -5.113eV) with three $As(OH)_3$ molecules is less than the three times adsorption energy of (110)-As(I) (E_{ad}=-2.401 eV) with one

129 $As(OH)_3$ molecule. Averaged by the number of $As(OH)_3$ molecules in adsorption energy $\overline{E}_{ad}$, it is found that the

130 $\overline{E}_{ad}$ of (100)-3As(III) or (110)-3As(III) is the smallest one among them. So the saturated concentration is

131 harmful to the As ions removal capability by MnO_2 bulk materials. Considering the periodic symmetry, the

132 maximum removal capacity of (110) bulk surface is quadruple to that of the (110)-As(I), which is equal to 180.00

133 mg/g. Although their adsorption energies don't strictly increase by multiple, the E_{ad} value is negative. So their

134 maximum adsorption capacity of (100) and (110) bulk surface can be increased in some concentration. In short,

135 the trend of adsorption energy for (100) or (100)-$As(OH)_3$ system, which becomes gentle along with the increased

136 concentration of As ions, indicates that the As removal capacity of MnO_2 bulk materials has a maximum value.

137 This point has been proved by the experimental (Zhang and Sun 2013; Ge et al. 2016; Camacho et al. 2011) and

138 theoretical (Luo et al. 2018) results. Comparing the same concentration of $As(OH)_3$ on (100) or (110) bulk surface,

139 the adsorption ability and capacity of $As(OH)_3$ molecules on (100) bulk surface is indeed stronger than that on

140 (110) bulk surface, which is also consistent with previous reports (Luo et al. 2018; Selvakumar et al. 2014).

141 **Table 1** Adsorption energy E_{ad} of $As(OH)_3$ molecules on (100), (110) and [(100×110)] models in aqueous solution.

Miller Index	Models	$E_{As+surface}$(eV)	$E_{surface}$(eV)	E_{ad}(eV)
(100)	(100)-As(I)	-97939.206	-93870.230	-2.641
	(100)-2As(II)	-101539.167	-93870.230	-6.050
	(100)-3As(III)	-103726.716	-93870.230	-6.396
(110)	(110)-As(I)	-74467.344	-70398.608	-2.401
	(110)-2As(II)	-78066.387	-70398.608	-4.892
	(110)-3As(III)	-80253.811	-70398.608	-5.113
[(100×110)]	[(100×110)]-As(I)	-75643.896	-71574.902	-2.659
	[(100×110)]-As(II)	-75643.683	-71574.902	-2.446
	[(100×110)]-As(III)	-75644.829	-71574.902	-3.592
	[(100×110)]-2As(I-II)	-78772.601	-71574.902	-4.595
	[(100×110)]-2As(I-III)	-78773.485	-71574.902	-5.479
	[(100×110)]-2As(II-III)	-78773.765	-71574.902	-5.759
	[(100×110)]-3As(III)	-83311.562	-71574.902	-7.438
	[(100×110)]-4As(IV)	-85499.646	-71574.902	-8.323
	[(100×110)]-5As(V)	-87686.654	-71574.902	-8.129

142 ## **3.2** Removal ability of nano-surface

143 As well known the α-MnO_2 bulk materials show limited adsorption capacity of toxic ions in water, which is

144 originated from their small surface area (Zhang and Sun 2013). However, the α-MnO_2 nanomaterials have

145 excellent adsorption and oxidation properties for their large specific surface area and many active sites (Thanh et

146 al. 2012). But the internal influence of nanometer effect is still mysterious. In the next part, the effect of

147 nano-surface on the adsorption performance of α-MnO_2 nanomaterials to As ions is discussed deeply by
148 microfacet model. All of the MnO_2-$As(OH)_3$ microfacet models are shown in Fig. 1c and Fig. S1. The results are
149 presented in Table 1. Compared with different adsorbed sites along α-MnO_2 microfacet layer, an $As(OH)_3$
150 molecule adsorbed on (100) plane of [(100×110)] was labeled by No.I, No.II and on (110) plane labeled by No.III.
151 When an $As(OH)_3$ molecule is adsorbed on (100) plane in [(100×110)]-As(III), its adsorption energy E_{ad} is equal
152 to -3.592 eV, which is lower than that of (100)-As(I) (E_{ad} = -2.641 eV) bulk surface. The adsorption energies E_{ad}
153 are equal to -2.446 eV or -2.659 eV when an $As(OH)_3$ molecule is adsorbed on (100) plane in [(100×110)]-As(II)
154 or [(100×110)]-As(I), which is larger than that of [(100×110)]-As(III). Although their adsorption concentration of
155 $As(OH)_3$ molecules is 24 mg/g, their different adsorption energies are mainly due to different active sites in MnO_2
156 nanostructure. Then the adsorption ability of $As(OH)_3$ molecules on MnO_2 nano-surface is better than that on
157 MnO_2 bulk surface due to the nanometer effect, which is consistent with experimental results that the MnO_2
158 nanomaterials have better catalytic performance than the bulk materials (Luo et al. 2018; Selvakumar et al. 2014).
159 Such conclusion verifies further that it is a good way to reveal the nanometer effect through microfacet model.

160 When the concentration of $As(OH)_3$ molecules increases to double times as 48 mg/g, its adsorption energy of
161 [(100×110)]-2As(II) is equal to -5.479 eV (Fig.1c and Fig.S1j), which is lower than the E_{ad} of [(100×110)]-As(III).
162 When the concentration of $As(OH)_3$ molecules increase to triple times as 72 mg/g, its absorption energy of
163 [(100×110)]-3As(III) is equal to -7.438 eV, which is lower than that of the same adsorption sites on (100) (E_{ad}=
164 -6.396 eV) or (110) (E_{ad}=-5.113 eV) bulk surface. These changes mean two or three $As(OH)_3$ molecules adsorbed
165 on [(100×110)] microfacet enhance their common adsorptive capacity. As the concentration of $As(OH)_3$
166 molecules increase to four or five times, the E_{ad} of [(100×110)]-4As(IV) or [(100×110)]-5As(V) decreases to
167 -8.323 eV or -8.129 eV, respectively. Their small difference in adsorption energies (ΔE_{ad}=0.194 eV) originates
168 from the similar adsorbing sites for $As(OH)_3$ on MnO_2 surface layer in aqueous solution (Fig. 1c). Analyzed the
169 Mn atoms along the surface layer of [(100×110)], it is found that there exist three adsorbed sites. Considering the
170 periodic symmetry of microfacet model, the maximum adsorption capacity of [(100×110)] is sextuple of
171 [(100×110)]-As(I), which is equal to 192 mg/g. It is larger than the maximum experimental value of 117 mg/g
172 (Luo et al. 2018). Their difference in maximum adsorption capacity comes from many factors, such as aqueous
173 solution environment, size of nanomaterials, pH and so on.

174 Systematically analyzing the adsorption abilities of (100), (110) bulk surface and [(100×110)] microfacet
175 model in aqueous solution to arsenic ions, it is found that the adhesion energies increase significantly at first, and
176 then slow down along with the increased concentration. Such a trend is consistent with previous experimental
177 studies (Thanh et al. 2012; Ge et al. 2016). This phenomenon is due to the saturation of adsorption sites and

existence of undisturbed arsenic ions (Fig. 1). Supposing all of the active sites of Mn atoms bonding with As ions, the saturated adsorption capability of [(100×110)] nanostructure is 192 mg/g, which is larger than that of (100) and (110) bulk surface. And to the same concentration of As ions, the adsorption energy of [(100×110)]-As system is lower than the corresponding (100) or (110) bulk surface. Their difference is only in the corner nanostructure of [(100×110)] nano-surface, which is not appeared in bulk surface. So the nanometer effect plays vital role in the removal process of As ions in aqueous solution by nanomaterials.

3.3 Electrostatic potential

The difference in adsorbability between MnO_2 bulk surface and nano-surface originates basically from their covalent electrons. Although experimental results have proved that the adsorption performance of MnO_2 nanomaterials is better than that of MnO_2 bulk materials (Thanh et al. 2013), detailed nanometer effect acting on the catalytic process of $As(OH)_3$ on MnO_2 in aqueous solution still keep mysterious. Patwardhan et al. (2012) have proved that the electrostatic attraction contributes to adsorption and bonding through experiments and simulation analysis. Thus, the electrostatic potential of arsenic adsorbed on (100), (110) and [(100×110)] was calculated carefully as showed in Fig. 2, Fig. 3 and Fig. S3, wherein the electrostatic potentials range from blue to white to red means that their values range from small to large. The average electrostatic potential of a unit cell along with the Z direction is shown in Fig. 2 and Fig. 3. In order to visually and systematically study the electrostatic attraction of all the MnO_2 bulk surface and nano-surface, the difference value (ΔV) of electrostatic potential between MnO_2 surface layer and $As(OH)_3$ molecule is calculated in all simulated arsenic adsorption models. It is found that the electrostatic potential between the oxygen atom in $As(OH)_3$ molecule and the manganese atom in MnO_2 surface layer is very large (electrostatic potential region is red), which means they are bonded strongly with each other (Fig. S3). Furthermore all of the electrostatic potentials of As, Mn and H elements are positive and that of O^{2-} is negative. So the $As(OH)_3$ molecules prefer to bond with OH^- to form $As(OH)_4$. The electrostatic potential of H_2O is very small. From Fig. 3, it is found that all of the electrostatic potential of MnO_2 no matter in bulk surface or microfacet is larger than the arsenite molecule. So the ability of electrons gain for Mn atom is much more powerful than that of As atom. Then Mn element performs oxidability and arsenic element performs reducibility. When the $As(OH)_3$ molecules adsorbed on MnO_2, the Mn^{4+} is reduced into Mn^{3+} and As^{3+} is oxidized into As^{4+} or As^{5+}. Youmbi and Calvayrac (2014) have shown that large adsorption capacity comes from the large difference in electrostatic potential value ΔV of the terminal layer and adsorbent layers. The trend of ΔV in (100) and (110) bulk surface along with different arsenic concentration follows as : $\Delta V_{((100)\text{-}3As(III))}$=1.029 eV > $\Delta V_{((100)\text{-}2As(II))}$=1.015 eV > $\Delta V_{((100)\text{-}As(I))}$=0.844 eV, $\Delta V_{((110)\text{-}3As(III))}$=0.679 eV >

$\Delta V_{((110)\text{-}2As(II))}$=0.536eV > $\Delta V_{((110)\text{-}As(I))}$=0.489 eV in Fig.2. The trend of ΔV in [(100×110)] microfacet along with different arsenic concentration is:$\Delta V_{([(100\times110)]\text{-}5As(V))}$=0.163 eV > $\Delta V_{([(100\times110)]\text{-}4As(IV))}$=0.142 eV > $\Delta V_{([(100\times110)]\text{-}3As(III))}$=0.121 eV > $\Delta V_{([(100\times110)]\text{-}As(III))}$=0.117 eV > $\Delta V_{([(100\times110)]\text{-}2As(II))}$=0.107 eV > $\Delta V_{([(100\times110)]\text{-}As(I))}$=0.105 eV > $\Delta V_{([(100\times110)]\text{-}As(II))}$=0.089 eV. These phenomenas show that the higher the concentration of $As(OH)_3$ molecule in aqueous solution lead to the stronger the electrostatic attraction of (100), (110) and [(100×110)] surface, which is basically consistent with the trend of their absorption energy. Previous papers (Xin et al. 2015; Praveena et al. 2014) confirm that large electrostatic potential values can lead to a strong electrostatic attraction, which plays an important role in physicochemical properties. However such conclusion is only got by bulk surface method, which doesn't consider the nanometer effect. In this paper, it is found that the electrostatic potential values in [(100×110)]-As nano-surface system is smaller than that in (100) or (110)-As bulk surface system, which is contrary to their trend in adsorption energy at the same concentration of As ions. Their only difference is originated from their geometric configurations whether containing nanostructure. Then the reason for [(100×110)]-As system possessing large adsorption energy with small electrostatic potential values is only derived from the influence of nanometer effect in [(100×110)] nano-surface. Small electrostatic potential values will be more beneficial to enhance the removal capability of As ions on MnO_2 nanomaterials. That may be a reason why MnO_2 nanomaterials have better catalytic activity than the bulk materials (Luo et al. 2018). Detailedly analyzed the product of $As(OH)_4$, which is only produced in [(100×110)] microfacet (Fig. 3e~g and Fig. S3k~m), it is found that their difference value (ΔV′) of electrostatic potential is smaller than the corresponding concentration of $As(OH)_3$, which means the adsorbility of $As(OH)_4$ is weaker than that of $As(OH)_3$ on [(100×110)]. And the trend of ΔV′ for metastable $As(OH)_4$ molecule becomes more and more small along with the addition of $As(OH)_3$ concentration. So the increased concentration of As ions weakens the adsorption ability of $As(OH)_4$ molecule on α-MnO_2 nanostructure. And the nanometer effect can promote the produce of transitional product $As(OH)_4$ molecule, which is also beneficial to enhance the removal capability of As ions on MnO_2 nanomaterials.

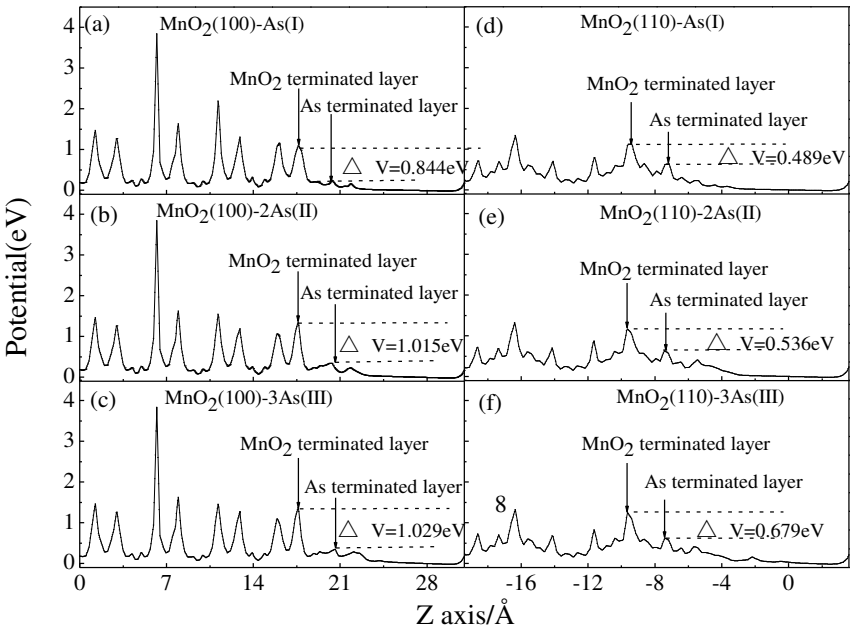

Fig. 2 Electrostatic potential along Z axis direction of different $As(OH)_3$molecules adsorbed on (100) and (110) bulk surface models.

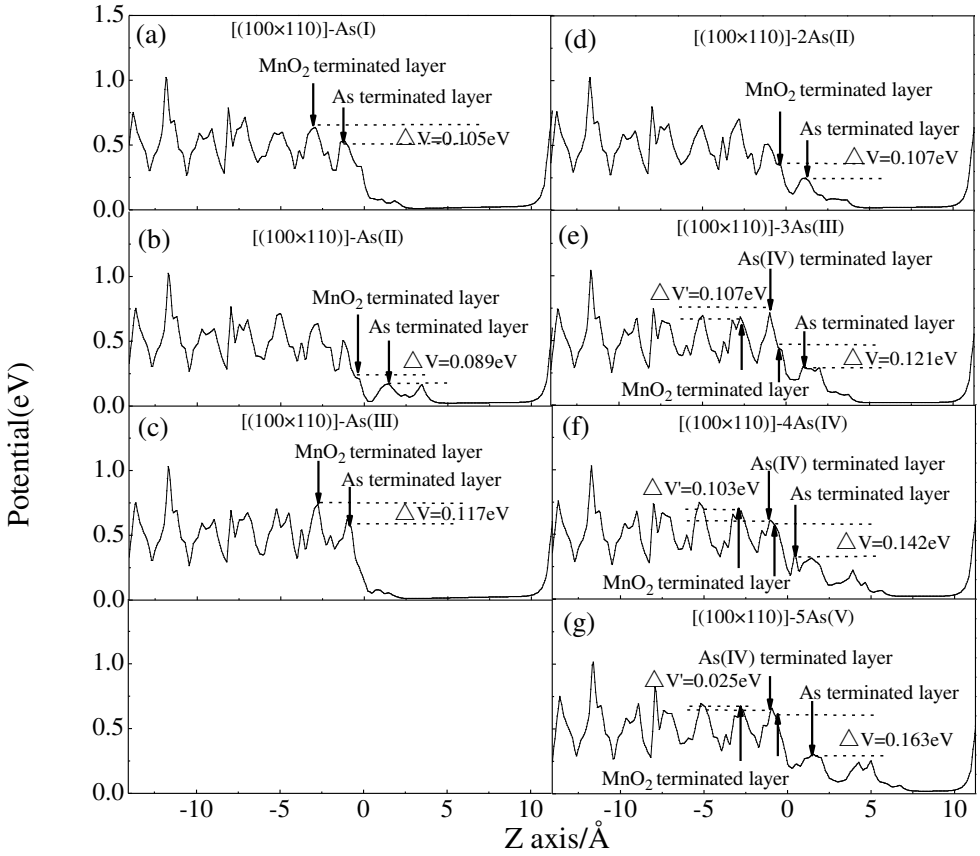

Fig. 3 Electrostatic potential along Z axis direction of different $As(OH)_3$molecules adsorbed on [(100×110)] microfacet surface models.

3.4 Catalytic mechanism

Until now, although the adsorbability of As ions on MnO_2 nanomaterials has been illuminated, the transformation process of $As(OH)_3$ (As^{3+})→$As(OH)_6$ (As^{5+}) molecule, especially the formation of trace metastable $As(OH)_4$ molecule has not been discovered clearly. The detailed catalytic mechanism of $As(OH)_3$ molecules on (100), (110) bulk surface and [(100×110)] nano-surface is analyzed systematically through the microscopic changes of geometry and electronic structure. For comparison, this paper only analyzes the same concentration of As ions adsorbed on MnO_2 models. And the original structure and electronic property of $As(OH)_3$, $As(OH)_6^-$ and H_2O molecules are calculated in Fig.4a~c. Their electronic properties are revealed by Mulliken population analysis (detailed explanation is shown in Supplement Information). The results are shown in Fig. 4 and Fig. S4.

For (100) and (110) bulk surface, it is found that their bond lengths of $As(OH)_3$ molecules have been changed significantly. The maximum bond length of $As(OH)_3$ molecule in its initial state is equal to 1.817 Å among three As-O bonds (Fig. 4a). However, it increases to 2.288 Å and 1.955 Å in (100)-3As(III) and (110)-3As(III) system respectively (Fig. 4d and e). Then their corresponding Mulliken populations are reduced from initial value 0.29 (Fig. S4a) to -0.04 (Fig. S4c) and 0.18 (Fig. S4d), which means a new bond formed

between Mn atom and OH^- hydroxyl of $As(OH)_3$ molecule. Then these new bonds can weaken the structural stability of $As(OH)_3$ molecules on α-MnO_2 bulk surface. This phenomenon confirms it is a chemisorption reaction between α-MnO_2 and $As(OH)_3$ molecules (Luo et al. 2018). Ans the transformation process (chemical reaction) of $As(OH)_3 \rightarrow As(OH)_6^-$ molecule can occur in (100) or (110)-As system, which is verified by experimental study (Lafferty et al. 2011).

For [(100×110)]-3As(III), [(100×110)]-4As(IV) and [(100×110)]-5As(V) models (Fig. 4f~h), it is found that their geometric structures of $As(OH)_3$ molecules at site (I') are also changed obviously. At the same time, its environmental H_2O molecules are decomposed into OH^- ion and H^+ ion clearly (Jung et al. 2015). That is because the bond lengths of H_2O molecules change from its initial state 0.974 Å (Fig. 4c) to 1.799 Å (Fig. 4f), 1.844 Å (Fig. 4g) and 2.276 Å (Fig. 4f) (marked via red color). Then some $As(OH)_3$ molecules bond with OH^- ions to form metastable $As(OH)_4$ molecules (labeled via (I)' in Fig. 4f~h). And the H^+ ions will adsorb on MnO_2 surface layer to form Mn-O-H clusters (Hasanpour et al. 2019), whose bonds are equal to 1.002 Å (Fig. 4f), 1.005 Å(Fig. 4g) and 1.007 Å (Fig. 4h) (marked via blue color). Such phenomenon doesn't appear in (100) or (110)-As system. Analyzing the geometric structure of precursor $As(OH)_4$ molecules at site (I') in a series of [(100×110)] models, it is shown that their largest bond lengths are 2.383 Å (Fig. 4f), 2.288 Å (Fig. 4g), 2.217 Å (Fig. 4h), and their Mulliken populations are -0.04 (Fig. S4e), -0.02 (Fig. S4f), -0.02 (Fig. S4g), respectively. Then the new product $As(OH)_4$ molecule is very weak, which is consistent with the experimental reports (Sun et al. 2015; Klaening et al. 1989). Comparing the morphology of $As(OH)_4$ molecule with $As(OH)_6^-$ molecule (Fig. 4b and c), it can be found that their geometric configurations are very similar to each other, especially to their hydroxyl groups. Sun et al. have pointed out that the As^{4+} ion is a very crucial intermediate in the catalytic process of $As^{3+} \rightarrow As^{5+}$ (Sun et al. 2015; Klaening et al. 1989). Therefore, we can infer that the $As(OH)_4$ molecule is the intermediate transition state oxide in the process of $As(OH)_3 \rightarrow As(OH)_6^-$ molecule. And the $As(OH)_4$ molecule intermediate appearing above [(100×110)] nano-surface is beneficial to As removal by MnO_2 nanomaterials. In other words the nanometer effect promotes the As removal ability of MnO_2 nanomaterials through a new way as producing much more intermediates.

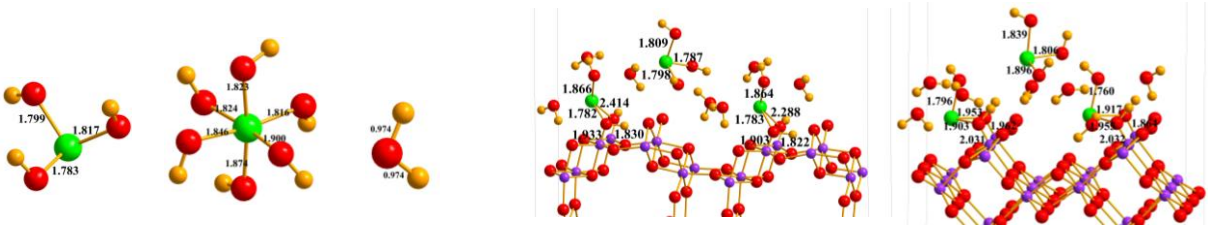

(a) $As(OH)_3$ (b) $As(OH)_6^-$ (c) H_2O (d) (100)-3As(III) (e) (110)-3As(III)

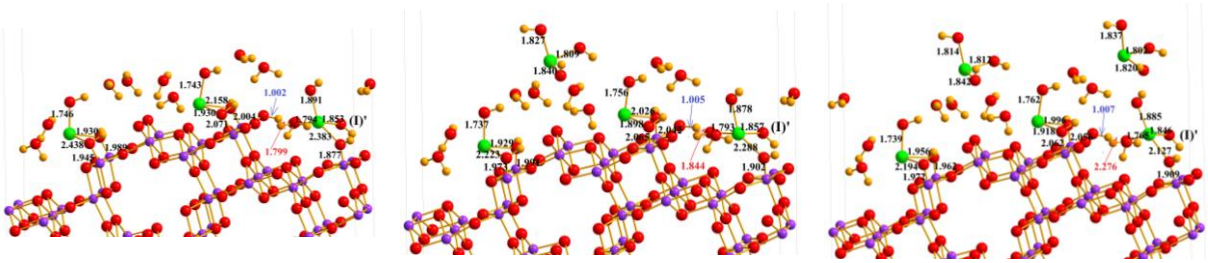

(f) [(100×110)]-3As(III) (g) [(100×110)]-4As(IV) (h) [(100×110)]-5As(V)

Fig. 4 Bond length of optimized model: (a) $As(OH)_3$ (b) $As(OH)_6^-$ (c) H_2O (d) (100)-3As(III), (e) (110)-3As(III), (f) [(100×110)]-3As(III), (g) [(100×110)]-4As(IV) and (h) [(100×110)]-5As(V).

3.5 Removing process

The purpose of removing As^{3+} in fact is to make it be oxidized into nontoxic As^{5+} (Luo et al. 2012). Then the formation rate of $As(OH)_6^-$ molecule plays a vital role in the application of MnO_2 nanomaterials. Experimental studies also show that some Mn^{3+} ions are resolved from matrix MnO_2 surface layer in the removing reaction of arsenic ions (Ge et al. 2016), which will lead to weight loss of MnO_2 nanomaterials. In this paper, we have proved the $As(OH)_4$ and $Mn(OH)^{2+}$ (Mn-O-H) molecules will only appear in MnO_2 nano-surface, wherein the $As(OH)_4$ molecule is an important transitional intermediate in $As(OH)_3 \rightarrow As(OH)_6^-$ process. As well known, there exist many hydroxyl groups in aqueous solution. Then the reduction process of $As(OH)_3 \rightarrow As(OH)_6^-$ molecule will exist two steps as $As(OH)_3 \rightarrow As(OH)_6^-$ or $As(OH)_3 \rightarrow As(OH)_4 \rightarrow As(OH)_6^-$. In the next part, the desorption process of arsenic ion in [(100×110)]-3As(III), [(100×110)]-4As(IV) and [(100×110)]-5As(V) system will be investigated by Climbing Image-Nudged Elastic Band (CI-NEB) way as shown in Fig.S5, which has been successfully applied to study desorption thermodynamics (Li et al. 2018; Zheng et al. 2017). The results are shown in Fig. 5. It is found the activation energies (ΔE_a) of $As(OH)_4$ molecules in the desorption process of [(100×110)]-3As(III), [(100×110)]-4As(IV), [(100×110)]-5As(V) system are equal to 2.332 eV, 2.732 eV and 4.733 eV, respectively. This results clearly show that the desorption reaction of $As(OH)_4$ molecules in [(100×110)]-3As(III) and [(100×110)]-4As(IV) is not hard due to their small activation energy, which may help us to have a deeper understanding of As(IV) ions in the experiment (Sun et al. 2015). As shown in Figs. 5d~f, the desorption energies of $As(OH)_6^-$ molecules in [(100×110)]-3As(III)', [(100×110)]-4As(IV)', [(100×110)]-5As(V)' system are equal to 3.138 eV, 3.936 eV and 5.084 eV, respectively, which is close to the activation energy of the corresponding $As(OH)_4$ molecular in desorption process. This phenomenon not only shows that the desorption ability of $As(OH)_6^-$ molecule is not very hard but also shows it has similar desorption ability with $As(OH)_4$ molecule, which is a stronger proof that $As(OH)_4$ molecule is the precursor state of $As(OH)_6^-$ molecule. No matter to $As(OH)_4$ or $As(OH)_6^-$ molecule, their desorption activation energy increases along with the increased concentration of As ions,

342 which means the free $As(OH)_3$ molecules can hinder the desorption reaction of $As(OH)_4$ or $As(OH)_6^-$ molecule.

343 In order to explore the dissolution ability of Mn^{3+} molecule influenced by the As ions, this paper takes
344 [(100×110)]-3As(III)" system as an example to study the desorption process of $Mn(OH)^{2+}$ molecule(Fig. S6). It is
345 found that the dissolution process of single $Mn(OH)^{2+}$ molecular (ΔE_a=11.479eV) in [(100×110)]-3As(III) is
346 much more difficult than the complex $As(OH)_3$-Mn^{3+} molecular (ΔE_a=5.447eV), which means the dissolution
347 ability of Mn^{3+} molecule becomes easy after $As(OH)_3$ adsorbed on the surface of MnO_2. Furthermore, in the
348 chemical reaction of $As(OH)_3 \rightarrow As(OH)_4^-$, the dissolution process of complex $As(OH)_4^-$-$Mn(OH)^{2+}$ has the
349 smallest activation energy (ΔE_a=4.602eV) among them. So the catalytic reaction of $As(OH)_3 \rightarrow As(OH)_6^-$ may
350 promote the dissolution ability of Mn^{3+} molecule, which is consistent with the experimental results (Ge et al.
351 2016). In the next paper, we will investigate the dissolution mechanism of Mn^{3+} molecule in the chemical reaction
352 of MnO_2 nanomaterials. According to their activation energy, it can be inferred that there exist two possible
353 desorption ways of $As(OH)_3$ molecule in aqueous solution: one is the catalytic reaction $As(OH)_3 \rightarrow As(OH)_6^-$
354 molecule at the low concentration, and another is the catalytic reaction $As(OH)_3 \rightarrow As(OH)_4$ accompanying with
355 derivative reduction reaction of $MnO_2 \rightarrow Mn(OH)^{2+}$. Nevertheless, the $As(OH)_4$ and $Mn(OH)^{2+}$ molecules don't
356 have stable structure, so the desorption process of $As(OH)_4$ molecule and $Mn(OH)^{2+}$ molecule in this state exhibits
357 $As(OH)_3 \rightarrow As(OH)_4 \rightarrow As(OH)_6^-$ and $MnO_2 \rightarrow Mn(OH)^{2+} \rightarrow Mn(OH)_3$ criteria respectively. So far the product of
358 $As(OH)_4$ molecule and the dissolution of Mn^{3+} ions are only found in [(100×110)] nano-surface, which almost
359 don't be observed in MnO_2 bulk surface. Then the nanometer effect although benefits to enhance the removal
360 capability of As ions through MnO_2 nanomaterials, it has bad influence to bring mass loss of nanomaterials. So the
361 nanostructure of catalytic materials needs to be optimized further.

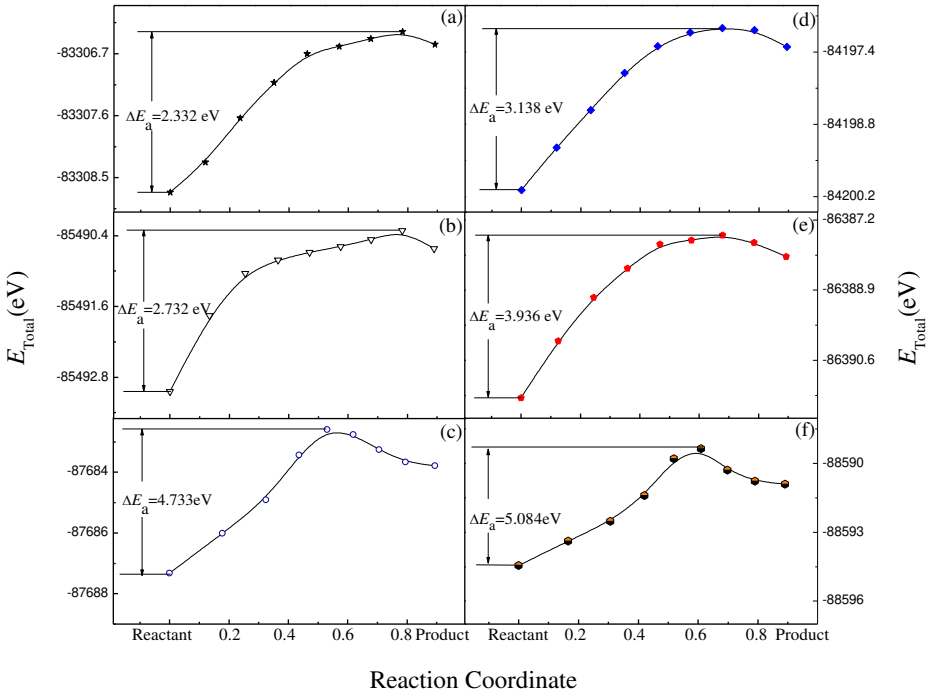

Fig. 5 Total energy E_{total} of desorption process for $Sb(OH)_4^-$ molecular on (a) [(100×110)]-3As(III) (b) [(100×110)]-4As(IV) (c) [(100×110)]-5As(V) and $Sb(OH)_6^-$ molecular on (d) [(100×110)]-3As(III)' (e) [(100×110)]-4As(IV)' (f) [(100×110)]-5As(V)' along [(100×110)] microfacet.

3.6 Discussion

The nanometer effect acting on the catalytic mechanism of arsenic ions adsorbed on α-MnO_2 nanomaterials can be extracted clearly. To simulate the performance of nanomaterials, this paper uses the microfacet model representing the geometric configuration of nano-surface compared with bulk surface concurrently. It is found that the trend of negative adsorption energies for $As(OH)_3$ molecules in bulk surface and microfacet system is basically decreased following the increasing concentration of As ions, which shows that the adsorption process is an exothermic reaction. The adsorption capacity of MnO_2 microfacet is larger than that of MnO_2 bulk surface, which is due to its much more active sites and less adsorption energy. A large difference in electrostatic potential of $As(OH)_3$ and MnO_2 layer attracts the adsorption process much easier. Wherein the nanometer effect provides small electrostatic potential of [(100×110)] nano-surface with large adsorption energy compared with bulk surface at the same concentration of As ions. Then in aqueous solution, there exist two possible desorption ways of $As(OH)_3$ molecule in aqueous solution. One is the direct reaction $As(OH)_3 \rightarrow As(OH)_6^-$ molecule at the low concentration. In this process, the H_2O is separated into H^+ and OH^-. The H^+ bond with Mn-O to form $Mn(OH)^{2+}$ along with the surface layer of MnO_2, which has small desorbed activation energy. And the $As(OH)_3$, which is catalyzed into $As(OH)_3^{2+}$, adsorbs hydroxyl OH^- to form $As(OH)_6^-$ molecule originated from their large

electrostatic potential. Such catalytic reaction can be observed both in bulk surface and nano-surface system. The other is the indirect process of $As(OH)_3 \rightarrow As(OH)_4 \rightarrow As(OH)_6^-$. At some active sites, the $As(OH)_3$ molecule is catalyzed into metastable precursor $As(OH)_4$ molecule to form $As(OH)_6^-$ molecule. Although the desorbed activation energy of $As(OH)_4$ molecule is smaller than that of $As(OH)_6^-$ molecule, the $As(OH)_4$ molecule is metastable and it is only produced at some special active sites. However such catalytic reaction can be easily occurred in nano-surface system. Compared with bulk materials, the nanomaterials have much more removal processes of As ions originated from nanometer effect. Then the removal mechanism of $As(OH)_3$ on MnO_2 nanomaterials can be extracted as shown in Fig. 6.

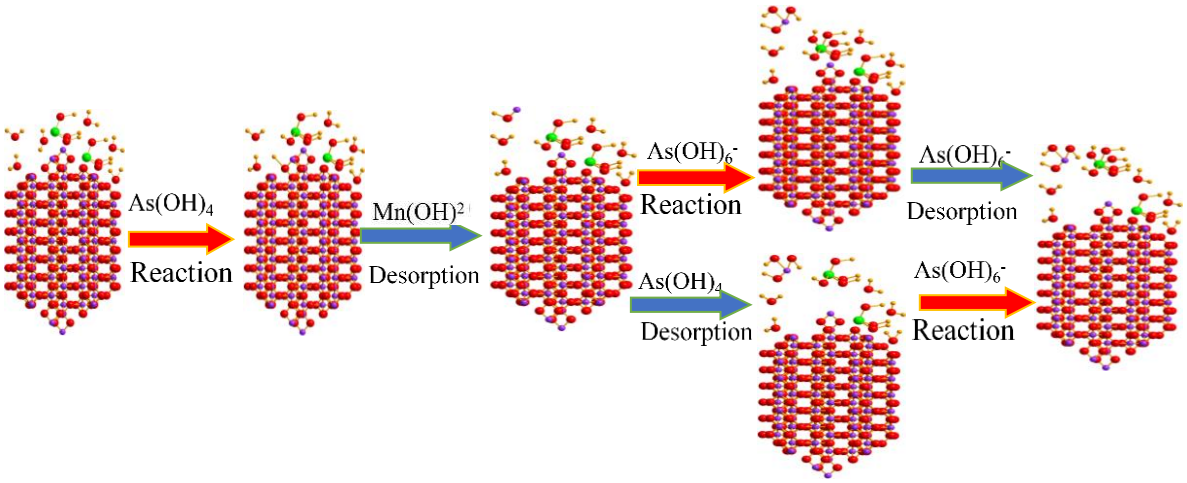

Fig. 6 Schematic diagram of the micromechanism of arsenic ions removal from aqueous solution via α-MnO_2 nanomaterials.

4. Conclusions

In summary, based on the theoretical analysis, the results showed that:

(1) The E_{ad} of $As(OH)_3$ molecules on α-MnO_2 bulk surface and microfacet are negative. These phenomena show the adsorbing reaction of $As(OH)_3$ molecules on α-MnO_2 nanomaterials is spontaneous and chemical reaction. With augment of $As(OH)_3$ molecules concentration in aqueous solution, the adsorption energy increases significantly at first, and then slow down. The maximum adsorption capacity of (100), (110) and [(100×110)] is equal to 78.67 mg/g, 180.00 mg/g and 192 mg/g, respectively.

(2) Electrostatic potential between the oxygen atom of $As(OH)_3$ molecule and the manganese atom of MnO_2 is very large, which means that they are bonded strongly with each other. The electrostatic potential of MnO_2 no matter in bulk surface or microfacet is larger than the arsenite molecule. Then Mn elements perform oxidability and arsenic elements perform reducibility. Difference in electrostatic potential value ΔV shows that the higher the concentration of $As(OH)_3$ molecule in aqueous solution lead to the stronger the electrostatic attraction of (100), (110) and [(100×110)] surface.

(3) Bond lengths of $As(OH)_3$ molecules on (100) and (110) bulk surface model have been changed from its initial state(1.817 Å) to 2.288 Å and 1.955 Å respectively. Their corresponding Mulliken population is reduced from an initial value 0.29 to -0.04 and 0.18. The $As(OH)_3$ molecule adsorbed at site (I') of [(100×110)] microfacet, a new bond is formed between an OH^- ion and an $As(OH)_3$ molecule to form metastable $As(OH)_4$ structure. An H^+ ion also adsorbed on MnO_2 to form Mn-O-H. Such phenomenon is due to the bond length of H_2O molecule changes from the initial state 0.974 Å to maximum value 2.276 Å.

(4) The activation energies in the desorption reaction of $As(OH)_4$ molecule on [(100 × 110)] are equal to 2.332 eV, 2.732 eV and 4.733 eV, respectively, and that of $As(OH)_6^-$ molecule are equal to 3.138 eV, 3.936 eV and 5.084 eV, respectively. Then the removal of arsenic from aqueous solution via α-MnO_2 nanomaterials follows $As(OH)_3 \rightarrow As(OH)_4 \rightarrow As(OH)_6^-$ and $MnO_2 \rightarrow Mn(OH)^{2+} \rightarrow Mn(OH)_3$. The activation energy of $Mn(OH)^{2+}$ molecule in the dissolution process of [(100×110)] is 4.602 eV. These phenomena indicate that the desorption reaction of arsenic will induce the manganese ions dissolving.

Acknowledgment

This work was supported by the National Natural Science Foundation of China (Grant No. 51361026, 52071172), the Jiangxi Provincial Natural Science Foundation (Grant No.20202BABL204024), the Key Research & Developement Plan of Jiangxi Province (Grant No.20181ACH80009), and the Innovation special fund project funding of Jiangxi graduate (Grant No.YC2018-S357).

Authors' contributions

Guifa Li and Pengsen Zhao conceived and conducted experimental research, analyzed experimental data and drafted manuscripts. Lixia Yang, Yongxiang Geng and Ping Peng provide expertise in adsorption catalysis. Haizhong Zheng initiated, conceived the experiment and wrote the manuscript; all the authors participated in the revision of the manuscript.

Data availability and materials

All the materials and data in this study can be found in this paper.

Compliance with ethical standards

Conflict of interest

The authors declare that they have no financial or personal relationship with any other person or organization that may unduly affect our work, and they have no known competing financial interests or personal relationships that could have appeared to influence the word reported in this paper.

Ethical Approval

The authors declare that they have no known competing financial interests or personal relationships that could have appeared to influence the word reported in this paper.

Consent to participate

All the authors volunteered to participate in this study.

Consent to publish

All the authors agreed to publish the manuscript.

References

Camacho LM, Parra RR, Deng S (2011) Arsenic removal from groundwater by MnO_2-modified natural clinoptilolite zeolite: Effects of pH and initial feed concentration. J Hazard Mater 189:286-293. https://doi.org/10.1016/j.jhazmat.2011.02.035

Chandra V, Park J, Chun Y, Lee JW, Hwang IC, Kim KS (2010) Water-dispersible magnetite-reduced graphene oxide composites for arsenic removal. ACS nano 4:3979-3986. https://doi.org/10.1021/nn1008897

Chen Z, Li G, Zheng H, Shu X, Zou J, Peng P (2017) Mechanism of surface effect and selective catalytic performance of MnO_2 nanorod: DFT+U study. Appl Surf Sci 420:205-213. https://doi.org/10.1016/j.apsusc.2017.05.141

Ge X, Liu J, Song X, Wang G, Zhang H, Zhang Y, Zhao H (2016) Hierarchical iron containing γ-MnO_2 hollow microspheres: a facile one-step synthesis and effective removal of As (III) via oxidation and adsorption. Chem Eng J 301:139-148. https://doi.org/10.1016/j.cej.2016.05.005

Gheju M, Balcu I, Mosoarca G (2016) Removal of Cr (VI) from aqueous solutions by adsorption on MnO_2. J

Hazard Mater 310:270-277. https://doi.org/10.1016/j.jhazmat.2016.02.042

Gupta K, Ghosh UC (2009) Arsenic removal using hydrous nanostructure iron (III)–titanium (IV) binary mixed oxide from aqueous solution. J Hazard Mater 161:884-892. https://doi.org/10.1016/j.jhazmat.2008.04.034

Hasanpour F, Saien J (2019) Incorporating Pb^{2+} Templates into the Crystalline Structure of MnO_2 Catalyst Supported on Monolith: Applications in H_2O_2 Decomposition. ACS Omega 4:16638-16650. https://doi.org/10.1021/acsomega.9b02565

Jiao F, Bruce PG (2007) Mesoporous Crystalline β-MnO_2—a Reversible Positive Electrode for Rechargeable Lithium Batteries. Adv Mater 19:657-660. https://doi.org/10.1002/adma.200602499

Johnson CS, Dees DW, Mansuetto MF, Thackeray MM, Vissers DR, Argyriou D, Loong CK, Christensen L (1997) Structural and electrochemical studies of α-manganese dioxide (α-MnO_2). J Power Sources 68:570-577. https://doi.org/10.1016/S0378-7753(96)02633-X

Jomova K, Jenisova Z, Feszterova M, Baros S, Liska J, Hudecova D, Rhodes CJ, Valko M (2011) Arsenic: toxicity, oxidative stress and human disease. J Appl Toxicol 31:95-107. https://doi.org/10.1002/jat.1649

Jung SJ, Lee JY, Hong S, Kim S (2005) Study of Adsorption and Decomposition of H_2O on Ge (100). J Phys Chem B 109:24445-24449. https://doi.org/10.1021/jp054415o

Klaening UK, Bielski BHJ, Sehested K (1989) Arsenic(IV). A pulse-radiolysis study. Inorg Chem 28:2717-2724. https://doi.org/10.1021/ic00313a007

Lafferty BJ, Ginder-Vogel M, Sparks DL (2011) Arsenite oxidation by a poorly-crystalline manganese oxide. 3. Arsenic and manganese desorption. Environ Sci Technol 45:9218-9223. https://doi.org/10.1021/es201281u

Li D, Shen G, Tang W, Liu H, Chen Y (2014) Large-scale synthesis of hierarchical MnO_2 for benzene catalytic oxidation. Particuology 14:71-75. https://doi.org/10.1016/j.partic.2013.06.010

Li G, Zhao P, Zheng H, Yang L, Lu S, Peng P (2018) Research on the removal mechanism of antimony on α-MnO_2 nanorod in aqueous solution: DFT+U method. J Hazard Mater 354:8-16. https://doi.org/10.1016/j.jhazmat.2018.04.055

Li Y, Xie H, Wang J, Chen L (2011) Preparation and electrochemical performances of α-MnO_2 nanorod for supercapacitor. Mater Lett 65:403-405. https://doi.org/10.1016/j.matlet.2010.10.048

Luo J, Meng X, Crittenden J, Qu J, Hu C, Liu H, Peng P (2018) Arsenic adsorption on α-MnO_2 nanofibers and the significance of (100) facet as compared with (110). Chem Eng J 331:492-500. https://doi.org/10.1016/j.cej.2017.08.123

Luo X, Wang C, Luo S, Dong R, Tu X, Zeng G (2012) Adsorption of As (III) and As (V) from water using magnetite Fe_3O_4-reduced graphite oxide–MnO_2 nanocomposites. Chem Eng J 187:45-52.

https://doi.org/10.1016/j.cej.2012.01.073

Mishra AK, Ramaprabhu S (2011) Functionalized graphene sheets for arsenic removal and desalination of sea water. Desalination 282:39-45. https://doi.org/10.1016/j.desal.2011.01.038

Patwardhan SV, Emami FS, Berry RJ, Jones SE, Naik RR, Deschaume O, Heinz H, Perry CC (2012) Chemistry of aqueous silica nanoparticle surfaces and the mechanism of selective peptide adsorption. J Am Chem Soc 134:6244-6256. https://doi.org/10.1021/ja211307u

Pessoa-Lopes M, Crespo JG, Velizarov S (2016) Arsenate removal from sulphate-containing water streams by an ion-exchange membrane process. Sep Purif Technol 166:125-134. https://doi.org/10.1016/j.seppur.2016.04.032

Praveena R, Sadasivam K, Deepha V, Sivakumar R (2014) Antioxidant potential of orientin: a combined experimental and DFT approach. J Mol Struct 1061:114-123. https://doi.org/10.1016/j.molstruc.2014.01.002

Reddy ALM, Shaijumon MM, Gowda SR, Ajayan PM (2009) Coaxial MnO_2/carbon nanotube array electrodes for high-performance lithium batteries. Nano lett 9:1002-1006. https://doi.org/10.1021/nl803081j

Segall MD, Lindan PJD, Probert MJ, Pickard CJ, Hasnip PJ, Clark SJ, Payne MC (2002) First-principles simulation: ideas, illustrations and the CASTEP code. J Phys-Condens Mat 14:2717. https://doi.org/10.1088/0953-8984/14/11/301

Selvakumar K, Kumar SMS, Thangamuthu R, Kruthika G, Murugan P (2014) Development of shape-engineered α-MnO_2 materials as bi-functional catalysts for oxygen evolution reaction and oxygen reduction reaction in alkaline medium. Int J Hydrogen Energ 39:21024-21036. https://doi.org/10.1016/j.ijhydene.2014.10.088

Song Z, Yan Z, Yang X, Bai H, Duan Y, Yang B, Leng L (2018) First principles density functional theory study of Pb doped α-MnO_2 catalytic materials. Chem Phys Lett 695:216-221. https://doi.org/10.1016/j.cplett.2018.02.023

Sun M, Zhang G, Qin Y, Cao M, Liu Y, Li J, Qu J, Liu H (2015) Redox conversion of chromium (VI) and arsenic (III) with the intermediates of chromium (V) and arsenic (IV) via AuPd/CNTs electrocatalysis in acid aqueous solution. Environ Sci Technol 49:9289-9297. https://doi.org/10.1021/acs.est.5b01759

Thanh DN, Singh M, Ulbrich P, Štěpánek F, Strnadová N (2012) As(V) removal from aqueous media using α-MnO_2 nanorods-impregnated laterite composite adsorbents. Mater Res Bull 47:42-50. https://doi.org/10.1016/j.materresbull.2011.10.004

Tompsett DA, Parker SC, Islam MS (2014a) Rutile (β-)MnO_2 surfaces and vacancy formation for high electrochemical and catalytic performance. J Am Chem Soc 136:1418-1426. https://doi.org/10.1021/ja4092962

515 Tompsett DA, Parker SC, Islam MS (2014b) Surface properties of α-MnO_2: relevance to catalytic and
516 supercapacitor behaviour. J Mater Chem A 2:15509-15518. https://doi.org/10.1039/C4TA00952E
517 Xiao F, Fang L, Li W, Wang D (2015) One-step synthesis of aluminum magnesium oxide nanocomposites for
518 simultaneous removal of arsenic and lead ions in water. RSC Adv 5:8190-8193.
519 https://doi.org/10.1039/C4RA13146K
520 Xiao W, Wang D, Lou XW (2009) Shape-controlled synthesis of MnO_2 nanostructures with enhanced
521 electrocatalytic activity for oxygen reduction. J Phys Chem C 114:1694-1700.
522 https://doi.org/10.1021/jp909386d
523 Xin Y, Hou SC, Xiang L, Yu YX (2015) Adsorption and substitution effects of Mg on the growth of calcium
524 sulfate hemihydrate: An ab initio DFT study. Appl Surf Sci 357:1552-1557.
525 https://doi.org/10.1016/j.apsusc.2015.09.223
526 Youmbi BS, Calvayrac F (2014) Structure of CoO (001) surface from DFT+ U calculations. Surf Sci 621:1-6.
527 https://doi.org/10.1016/j.susc.2013.10.012
528 Zhang M, He G, Pan G (2015) Binding mechanism of arsenate on rutile (1 1 0) and (0 0 1) planes studied using
529 grazing-incidence EXAFS measurement and DFT calculation. Chemosphere 122:199-205.
530 https://doi.org/10.1016/j.chemosphere.2014.11.053
531 Zhang T, Sun DD (2013) Removal of arsenic from water using multifunctional micro-/nano-structured MnO_2
532 spheres and microfiltration. Chem Eng J 225:271-279. https://doi.org/10.1016/j.cej.2013.04.001
533 Zheng H, Chen Z, Li G, Shu X, Peng P (2017) High-temperature corrosion mechanism of YSZ coatings subject to
534 calcium–magnesium–aluminosilicate (CMAS) deposits: first-principles calculations. Corros Sci 126:286-294.
535 https://doi.org/10.1016/j.corsci.2017.07.010

Figures

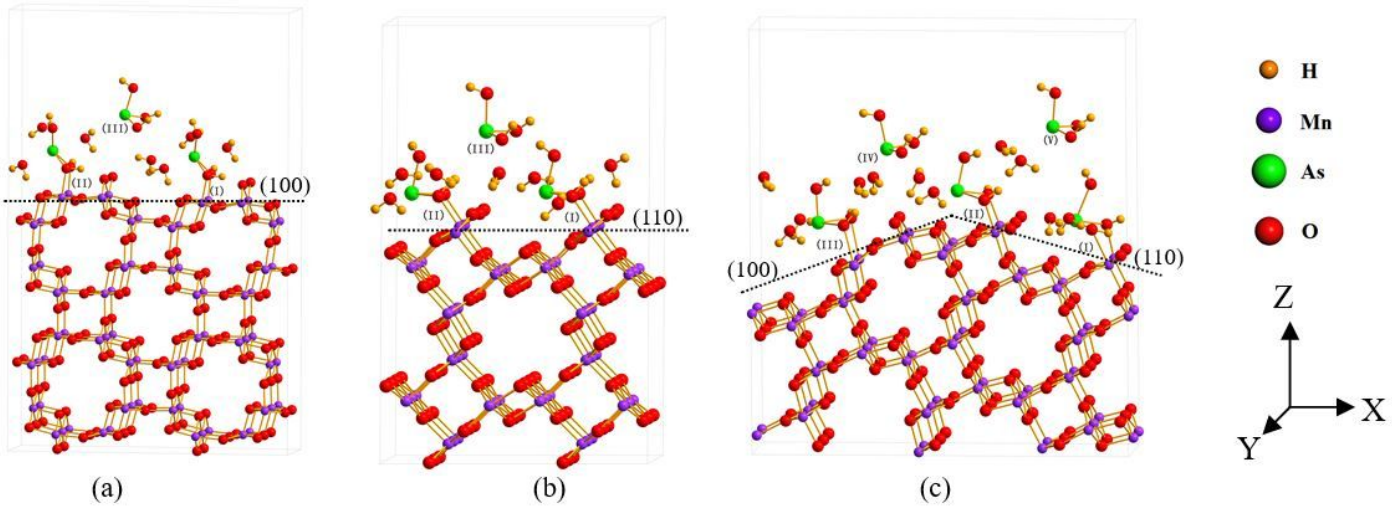

Figure 1

Adsorption models of As(OH)3 molecules with different concentration and sites on (a) (100), (b) (110) bulk surface and (c) [(100×110)] microfacet.

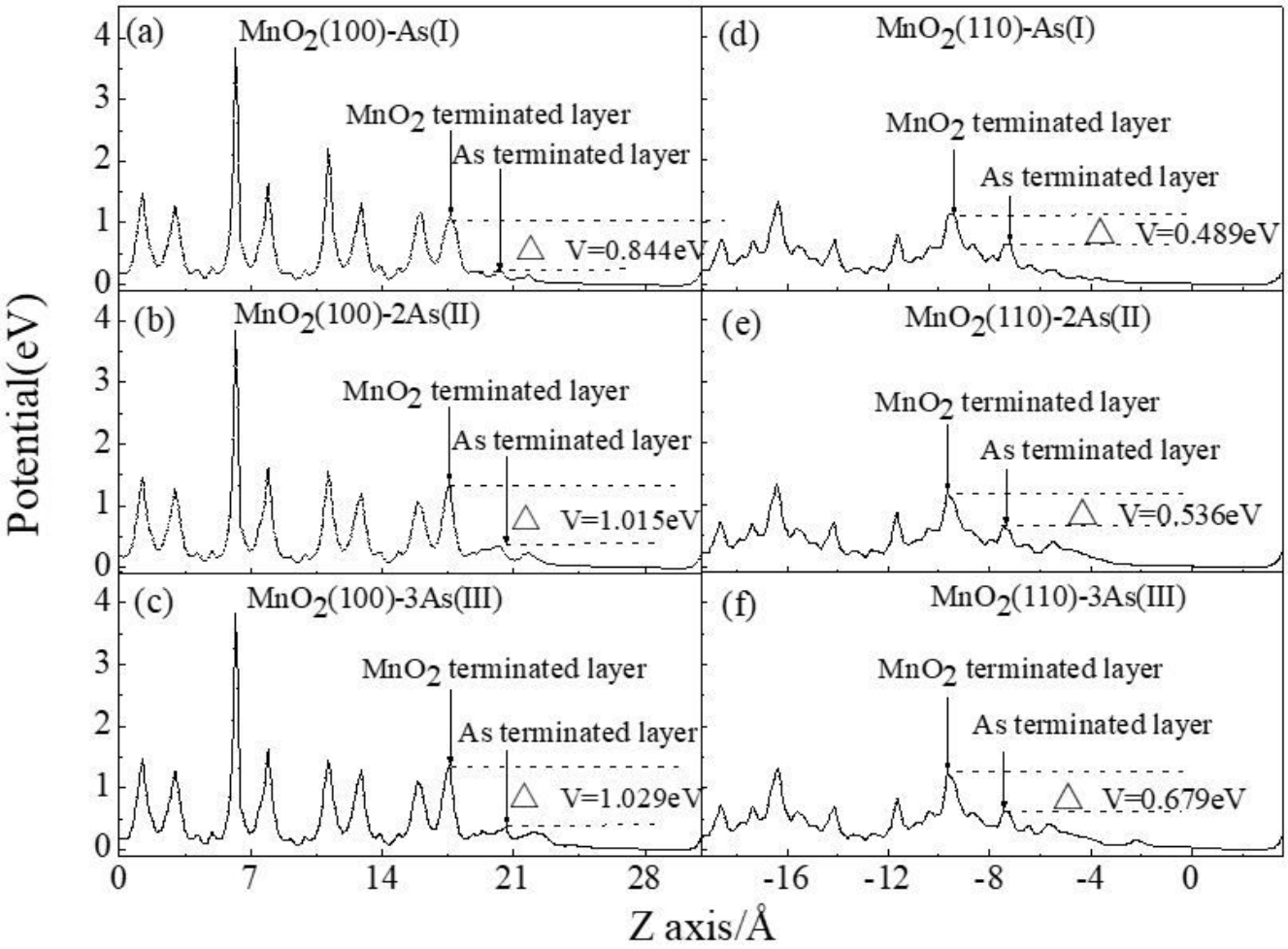

Figure 2

Electrostatic potential along Z axis direction of different As(OH)3molecules adsorbed on (100) and (110) bulk surface models.

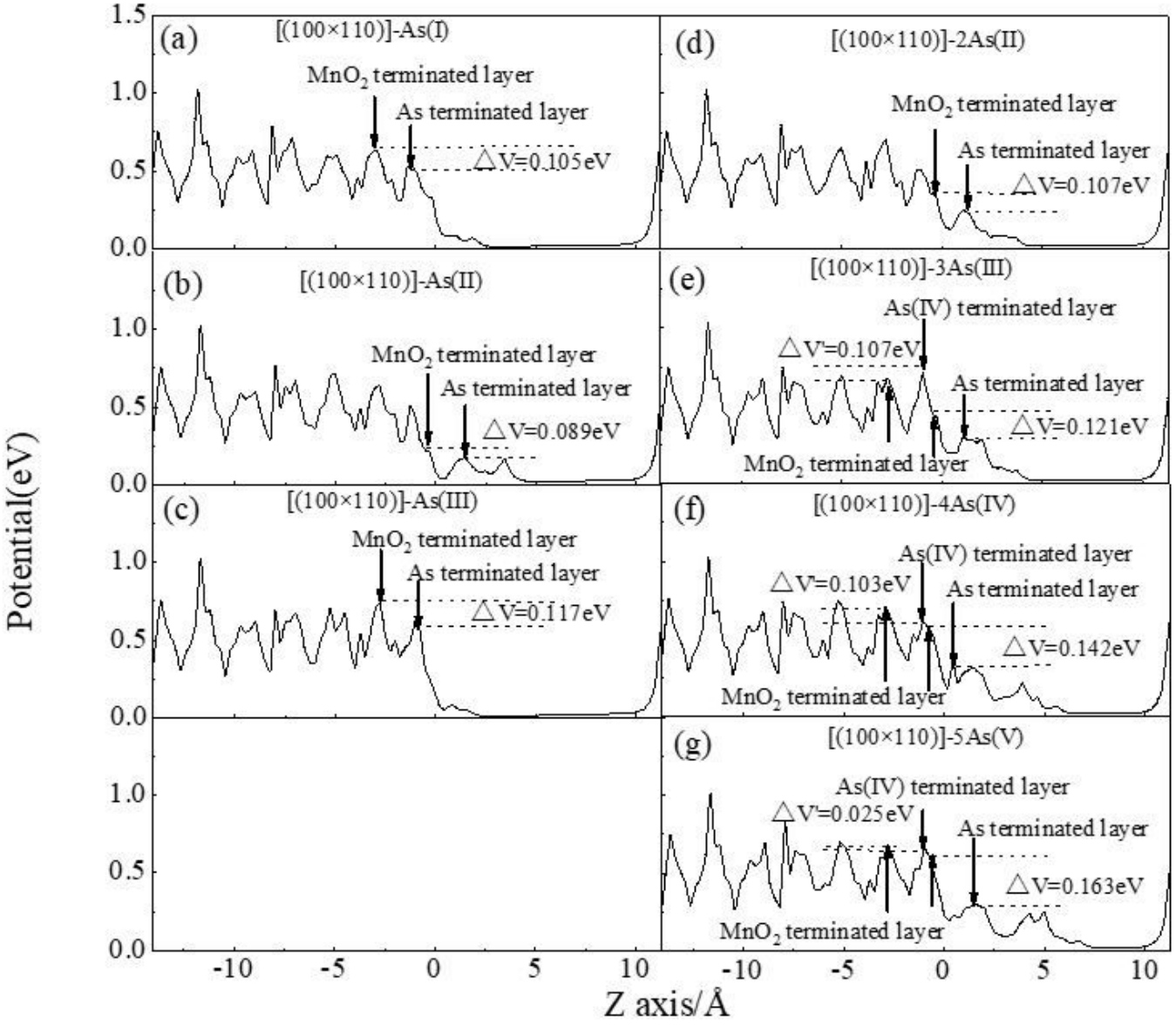

Figure 3

Electrostatic potential along Z axis direction of different As(OH)3molecules adsorbed on [(100×110)] microfacet surface models.

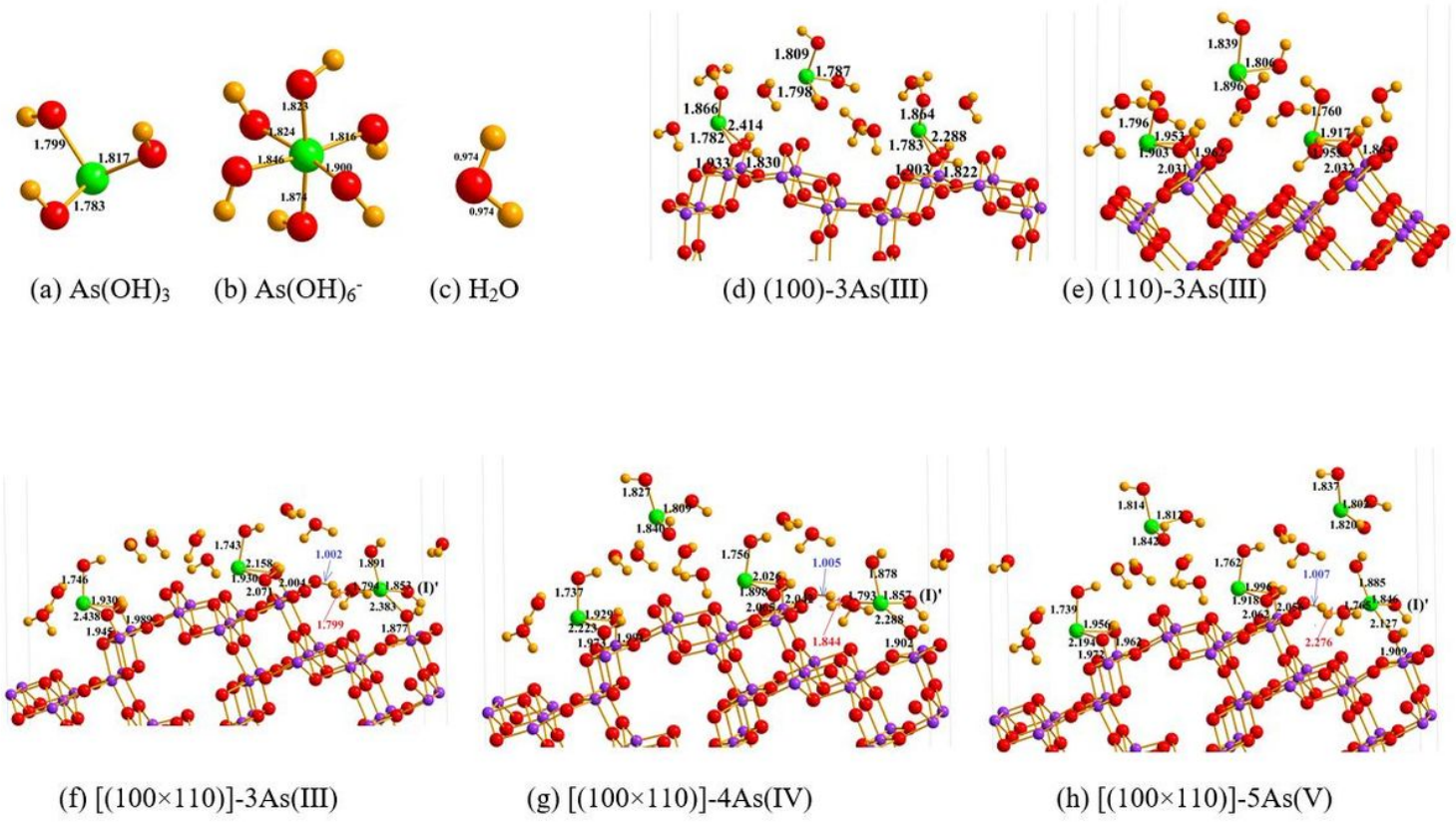

Figure 4

Bond length of optimized model: (a) As(OH)3 (b) As(OH)6- (c) H2O (d) (100)-3As(III), (e) (110)-3As(III), (f) [(100×110)]-3As(III), (g) [(100×110)]-4As(IV) and (h) [(100×110)]-5As(V).

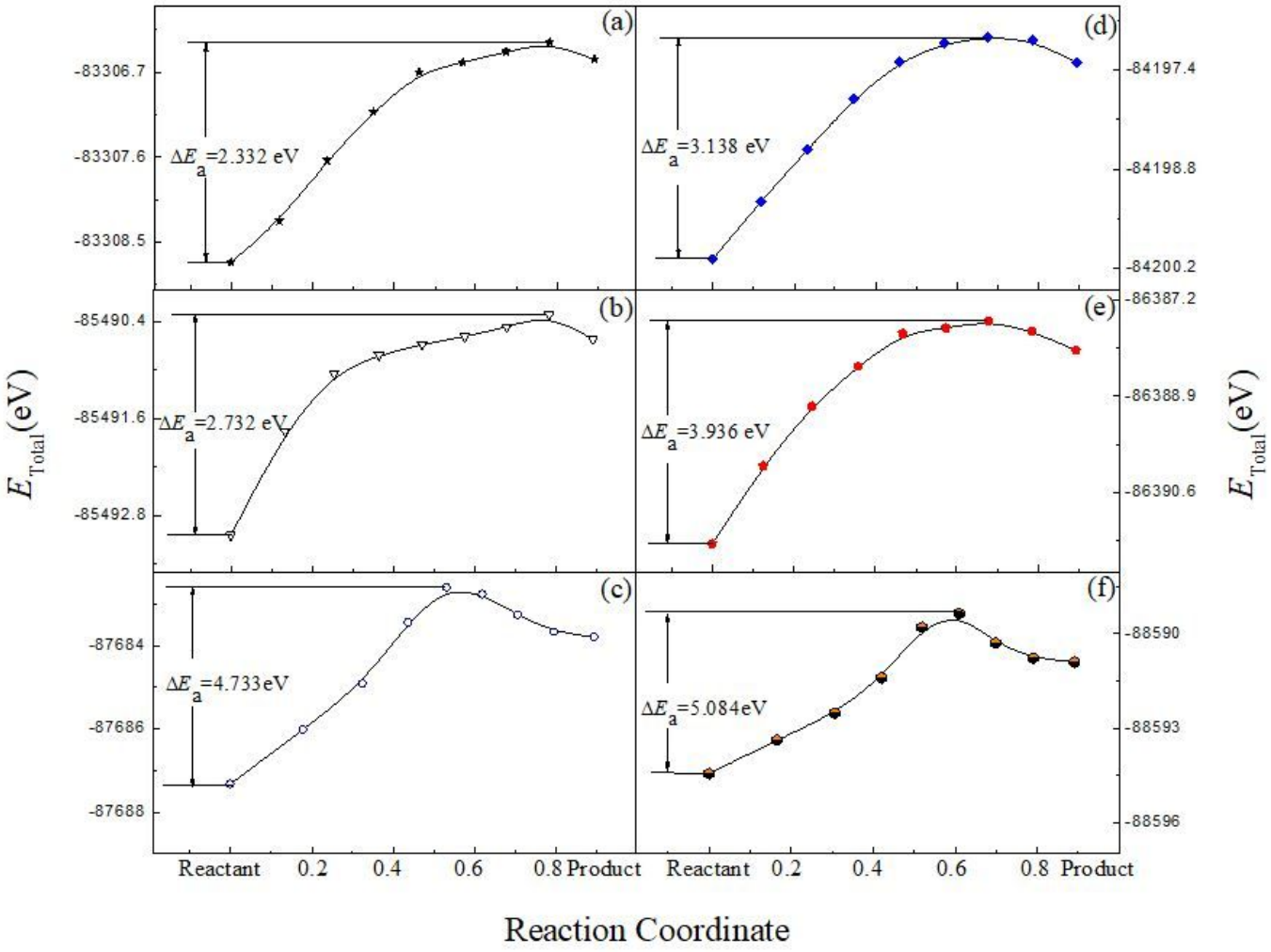

Figure 5

Total energy Etotal of desorption process for Sb(OH)4- molecular on (a) [(100×110)]-3As(III) (b) [(100×110)]-4As(IV) (c) [(100×110)]-5As(V) and Sb(OH)6- molecular on (d) [(100×110)]-3As(III)' (e) [(100×110)]-4As(IV)' (f) [(100×110)]-5As(V)' along [(100×110)] microfacet.

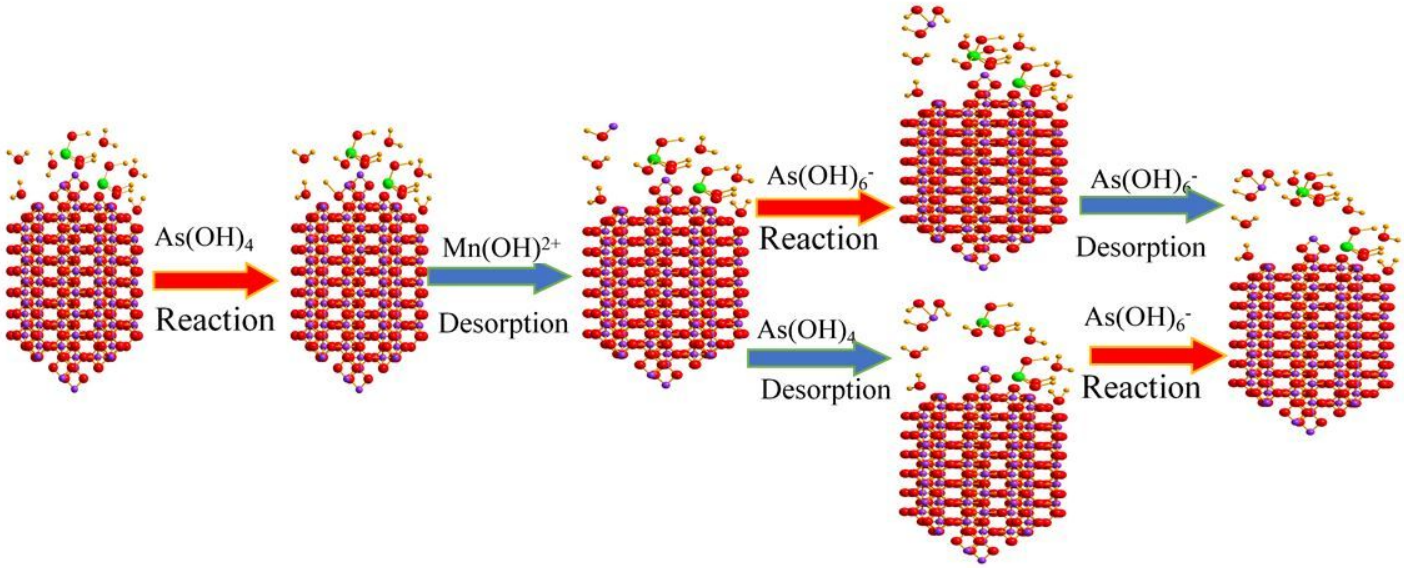

Figure 6

Schematic diagram of the micromechanism of arsenic ions removal from aqueous solution via α-MnO2 nanomaterials.

Supplementary Files

This is a list of supplementary files associated with this preprint. Click to download.

- SupplementaryMaterialzhaoVSI.doc